Effect of inertia in Rayleigh-Bénard convection

M. Breuer, S. Wessling, J. Schmalzl, and U. Hansen*
Institut für Geophysik, Westfälische Wilhelms-Universität Münster, D-48149 Münster, Germany
(Received 6 August 2003; revised manuscript received 7 October 2003; published 24 February 2004)

We have investigated the influence of the Prandtl number on the dynamics of high Rayleigh number thermal convection. A numerical parameter study in a three-dimensional Rayleigh-Bénard configuration was carried out, where we varied the Prandtl number between $10^{-3} \leqslant \mathrm{Pr} \leqslant 10^2$. The Rayleigh number was fixed at a value of $\mathrm{Ra} = 10^6$. Our main focus lay on the question how the value of the Prandtl number affects the spatial structure of the flow. We investigated the functional dependence of the Nusselt number and the Reynolds number and compared our results with a recent theoretical approach of Grossmann and Lohse [J. Fluid Mech. **407**, 27 (2000); Phys. Rev. Lett. **86**, 3316 (2001)].

DOI: 10.1103/PhysRevE.69.026302 PACS number(s): 47.27.Te, 92.60.Ek

I. INTRODUCTION

Vigorous thermal convection is a fundamental phenomenon, largely governing the dynamics of natural systems like the atmosphere, oceans, and planetary interiors. It also plays an important role in technical applications like process technology. The past years saw active research in the field where many efforts centered around scaling laws between the control parameter Rayleigh number Ra and the output parameters Nusselt number Nu and Reynolds number Re. While so far no universal scaling law for the Nusselt-Rayleigh number relation could be found [1] it became clear that an understanding of the output parameters on the other control parameter, i.e., the Prandtl number Pr is crucial to fully understand the dynamics. Systematic investigations on the influence of Pr on the flow dynamics were hampered by the relative difficulties to perform appropriate experiments in the laboratory. Also numerical approaches today still face considerable problems to deal with high Rayleigh number convection with varying Prandtl number. However, the situation has recently improved. Laboratory experiments using appropriate liquids and gases can span a significant range of Prandtl numbers [2–5]. Especially numerical studies have been applied to study effects of largely varying Prandtl numbers [6]. This is of special interest in the geophysical context, since the Prandtl number in different geophysical systems (e.g., for the molten Earth's core and the viscous Earth's mantle) ranges between rather extreme values (from 0.1 to virtual infinity for the specified systems). In particular recently a new theory was pushed forward by Grossmann and Lohse [7,8] making several predictions with respect to global output parameters but also with respect to the development of thermal and viscous boundary layers and their influence on the scaling laws. In the present study we have fixed the Rayleigh number to a value at 10^6 and have varied the Prandtl number in a range of $10^{-3} \leqslant \mathrm{Pr} \leqslant 10^2$. We analyze some assumptions forming the basis of the Grossmann-Lohse theory and show that their assumption of the type of the viscous boundary layer is not in accordance with our results. Nevertheless key predictions of the theory came out to be in close agreement with our results. And up to now widely overlooked property of the flow is the ratio of toroidal to total energy which is strongly decreasing with increasing Prandtl number. We consider this to be characteristic for the different type of dynamics at low and high Prandtl numbers.

II. MODEL AND NUMERICAL SETUP

We studied Rayleigh-Bénard convection of a Boussinesq fluid in a three-dimensional (3D) Cartesian domain by means of a numerical model. The describing set of equations, deduced from conservation of mass, energy, and momentum is given in nondimensional form by

$$1/\mathrm{Pr}(\partial_t \mathbf{u} + \mathbf{u}\cdot\boldsymbol{\nabla}\mathbf{u}) + \boldsymbol{\nabla} p - \boldsymbol{\nabla}^2 \mathbf{u} - \mathrm{Ra} T \mathbf{e}_z = 0, \tag{1}$$

$$\partial_t T + \mathbf{u}\cdot\boldsymbol{\nabla} T - \boldsymbol{\nabla}^2 T = 0, \tag{2}$$

$$\boldsymbol{\nabla}\cdot\mathbf{u} = 0, \tag{3}$$

where $\mathbf{u}$ is the velocity vector, p the pressure without the hydrostatic component, T denotes the temperature, and $\mathbf{e}_z$ is the unit vector in z direction. The equations have been made nondimensional using the height d of the box, the temperature difference $\Delta T = T_{bot} - T_{top}$ between the bottom and the top and the thermal diffusion time $t_\kappa = d^2/\kappa$. The similarity parameters, the Rayleigh number Ra and the Prandtl number Pr, are defined by

$$\mathrm{Ra} = \alpha g \Delta T d^3/\nu\kappa, \quad \mathrm{Pr} = \nu/\kappa, \tag{4}$$

where α is the thermal expansivity, g is the acceleration due to gravity, ν denotes the kinematic viscosity, and κ represents the thermal diffusivity. At the upper and lower surfaces we employed no-slip conditions for the velocity while the temperature was kept constant ($T_{bot} = 1, T_{top} = 0$). The sidewalls were adiabatic and free-slip conditions were adapted for the velocity. The aspect ratio was set to $A = 2$. In numerical experiments it is common to use free-slip conditions for the velocity field on the vertical walls in order to minimize sidewalls effects, in particular to avoid the generation of viscous boundary layers at the sidewalls (cf. Ref. [1]). The numerical integration of Eqs. (1)–(3) was performed by a finite volume multigrid method, with a time-stepping scheme,

*Electronic address: breuerm@earth.uni-muenster.de

based on an explicit Adams-Bashforth and the implicit Crank-Nicolson method. The solution method is essentially based on that of Trompert and Hansen [9], with some modifications described in Schmalzl *et al.* [6]. Due to the existence of strong vertical gradients of the temperature and velocity field near the upper and lower boundaries (cf. Sec. IV) one must assure that these boundary layers are appropriately resolved. Following Grötzbach [10] there should be at least 3–5 grid points in these boundary layers for sufficient accuracy. Our method allows for nonequidistant grids in vertical direction. The position of the grid points are defined by roots of Chebyshev polynomials,

$$z(i)=\frac{(z_{top}+z_{bot})}{2}-\frac{(z_{top}-z_{bot})}{2\cos(\pi b)}\times\cos\left[\pi\left(b+\frac{(i-1)(1-2b)}{NZ}\right)\right],$$

$$i=1,\ldots,NZ+1, \tag{5}$$

where NZ is the number of control volumes in the z direction and b controls the degree of the refinement. Most model runs were carried out on a $64\times64\times32$ grid. It turned out that grid refinement was necessary for Prandtl numbers less than 5 in order to fulfill the criterion mentioned above. In experiments with $\mathrm{Pr}\geqslant5$ boundary layers were accurately resolved by a uniform grid. In order to check our results for under-resolution we compared the temporal evolution of the Nusselt number for two grid configurations. For both, a low value of the Prandtl number [$\mathrm{Pr}=0.001$, Fig. 1(a)] and a higher value [$\mathrm{Pr}=30$, Fig. 1(b)], we monitored the evolution of the flow on a $64\times64\times32$ and on a finer grid consisting of $128\times128\times64$ nodes. In all cases the Rayleigh number was set to $\mathrm{Ra}=10^6$. Figures 1(a) and 1(b) display the time history of Nu. Clearly both resolutions provide satisfactory agreement. We conclude this also from the observation that the mean values of Nu, averaged over the time span shown in Fig. 1, deviate by less than 3% for both Prandtl numbers. Grötzbach [10] points out that specially Nu is a sensitive indicator of under-resolution. The close agreement of the mean values thus points towards proper resolution. Another useful test to check the results against under-resolution is to compare the Nusselt number, averaged over the depth of the fluid layer, $\mathrm{Nu}_{av}=\int_{z=0}^{1}dz(\langle wT\rangle_h-(\partial/\partial z)\langle T\rangle_h)$, with the Nusselt number at the upper surface, $\mathrm{Nu}_{top}=-(\partial/\partial z)\times\langle T\rangle_h|_{z=1}$ ($\langle\cdot\rangle_h$ denotes the horizontal mean). For proper resolution the time averaged values should yield the same result. In all runs we found the two values to be virtually identical, and thus this constraint to be well satisfied. For all model runs the conductive state with a superimposed temperature perturbation was employed as initial condition. The calculations were evolved until transients faded away and a statistically stationary state was reached. To do so the calculations were carried out for at least 70 large-eddy-turnover times (defined as $\tau=d/U_{rms}$ [11], U_{rms} being the root-mean-square velocity).

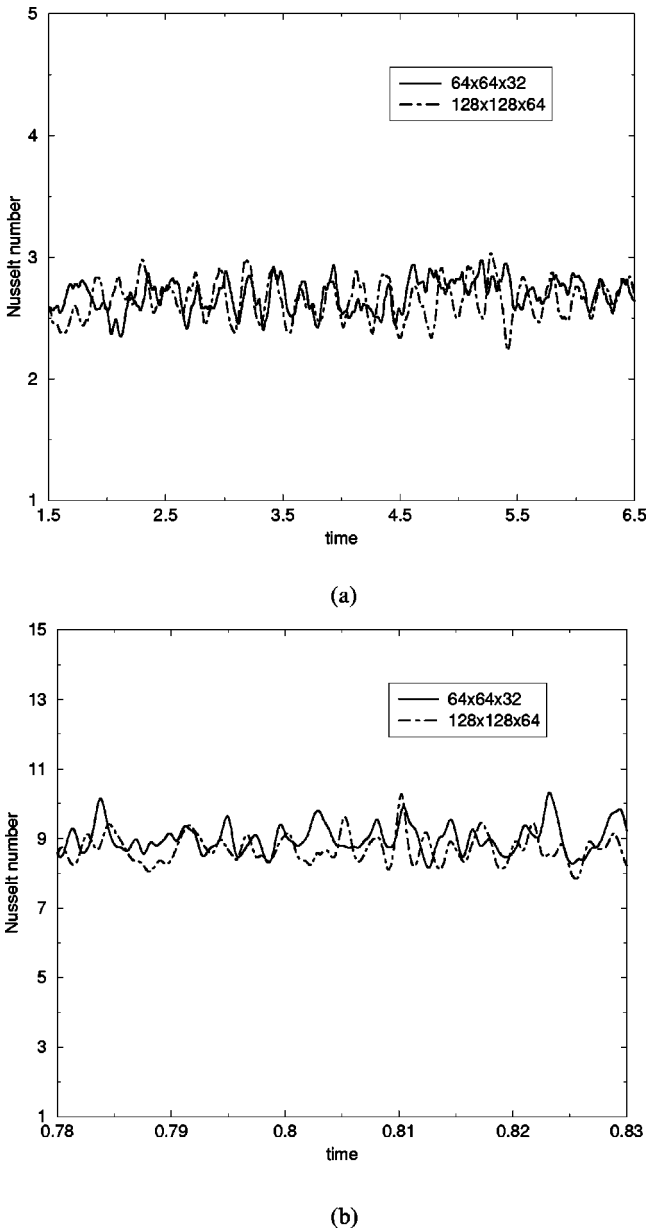

FIG. 1. The influence of the spatial resolution on the temporal evolution of the Nusselt number for (a) $\mathrm{Pr}=0.001$ and (b) $\mathrm{Pr}=30$. We compare runs developed on a $64\times64\times32$ grid against runs with a higher grid resolution of $128\times128\times64$.

III. SPATIAL STRUCTURE OF THE FLOW

In order to investigate the influence of the Prandtl number on the flow properties in thermal convection, we carried out a numerical parameter study in a three-dimensional Rayleigh-Bénard configuration with an aspect ratio of $A=2$, subject to rigid conditions at the upper and lower boundaries and stress-free sidewalls. The Rayleigh number was fixed at a value of $\mathrm{Ra}=10^6$, high enough to get strong time dependent flow dynamics. We varied the Prandtl number over a wide range from $\mathrm{Pr}=10^{-3}$ up to $\mathrm{Pr}=100$.

In order to explore the effect of inertia on convection it seems useful to first look at the spatial structure of the flow before applying more sophisticated diagnostics. Visualization

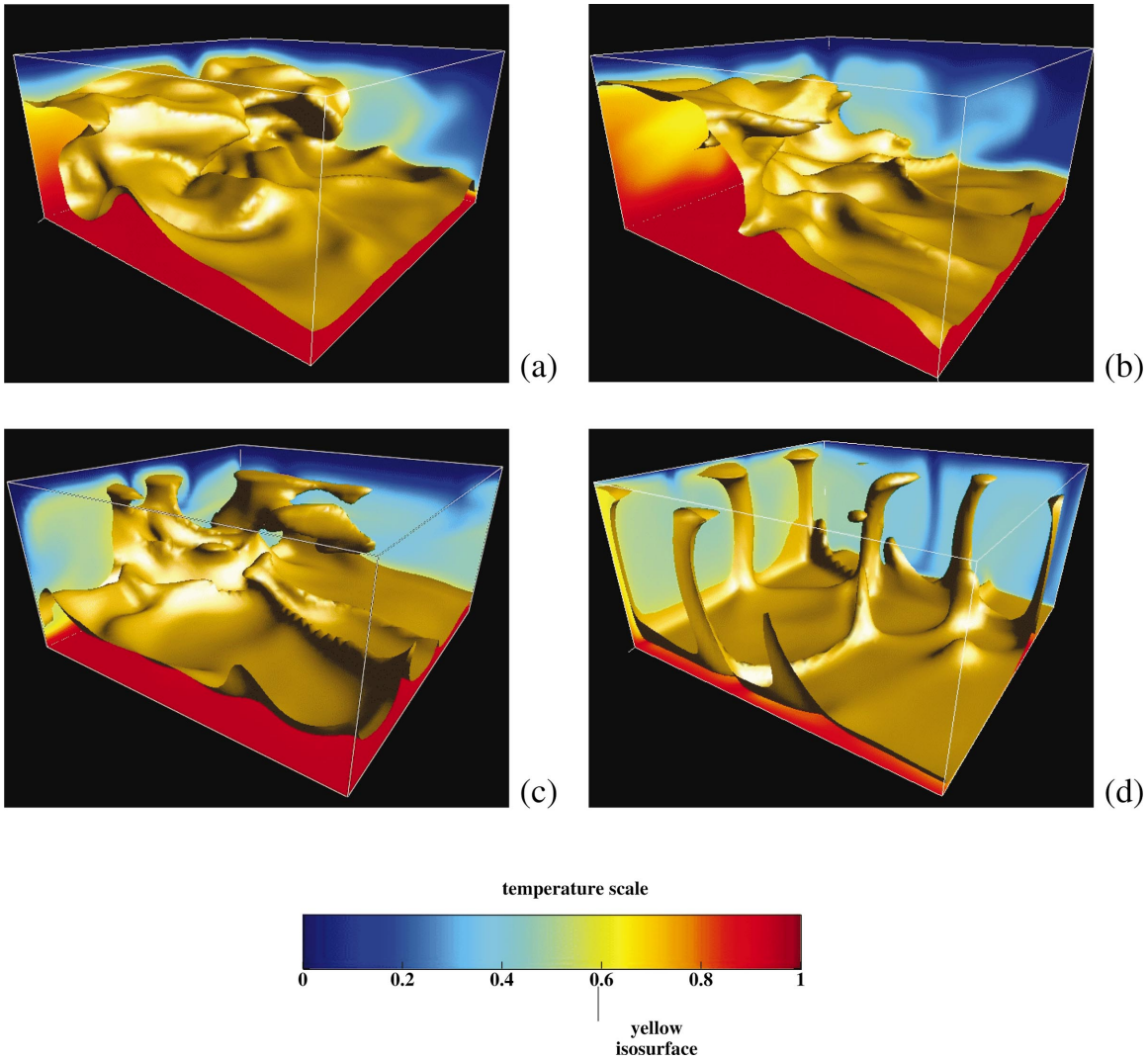

FIG. 2. (Color) Snapshots of the temperature field, illustrated by the temperature isosurface for the nondimensional value of $T=0.6$ and temperature cross sections at three side walls, for the values of the Prandtl number: (a) Pr$=0.025$, (b) Pr$=0.1$, (c) Pr$=1$, and (d) Pr $=100$.

is a powerful tool and the relative ease with which it can be used is certainly one of the advantages of numerical studies. In laboratory experiments visualization can be a formidable task. In Figs. 2(a)–2(d) snapshots of the temporal evolution of the temperature fields for four different values of the Prandtl number are shown [Pr$=0.025$ (a), 0.1 (b), 1 (c), 100 (d)]. Temperature is dimensionless and varies between $T=1$ at the bottom and $T=0$ at the top. We picked the $T=0.6$ isosurface because it nicely displays the structure of the warm up-wellings. Further, color coded cross sections of the temperature on three sidewalls illustrate the distribution of temperature. The down-welling currents behave symmetrically and are not shown here. On a first glance, we can identify some obvious differences in the thermal structure between low and high values of the Prandtl number. At low Prandtl numbers [Pr$=0.025$ and 0.1, Figs. 2(a) and 2(b)] a large-scale circulation develops, extending from one side of the box where an up-welling has developed to the down-welling at the opposite side. At a value of Pr$=1$ [Fig. 2(c)] plumelike structures have developed. They are, however, still pushed by the large-scale flow towards the sidewalls of the box. At Pr$=100$ [Fig. 2(d)] the plumes are fully developed and give rise to a multicellular structure of the flow. The largest scale of the flow is now given by the size of the cells rather than by the full length of the box. Our finding agrees well with the results of Verzicco and Camussi [12] who performed numerical experiments in a cylindrical cell. They also report a change from a large-scale flow dominated heat transport at low values of the Prandtl number to a regime at high Prandtl numbers where the heat transport is mainly due to thermal plumes. An experimental study revealing the dominance of thermal plumes with regard to heat transport at high Pr has been described by Ciliberto *et al.* [13].

To further investigate the thermal flow structure we have calculated the spatial temperature probability density function (PDF) for different values of the Prandtl number [Figs. 3(a)–3(d)]. The PDF's can be derived from the histogram of the spatial temperature distribution [14] with

$$pdf(T_i) \approx \frac{n_i}{N\Delta}, \tag{6}$$

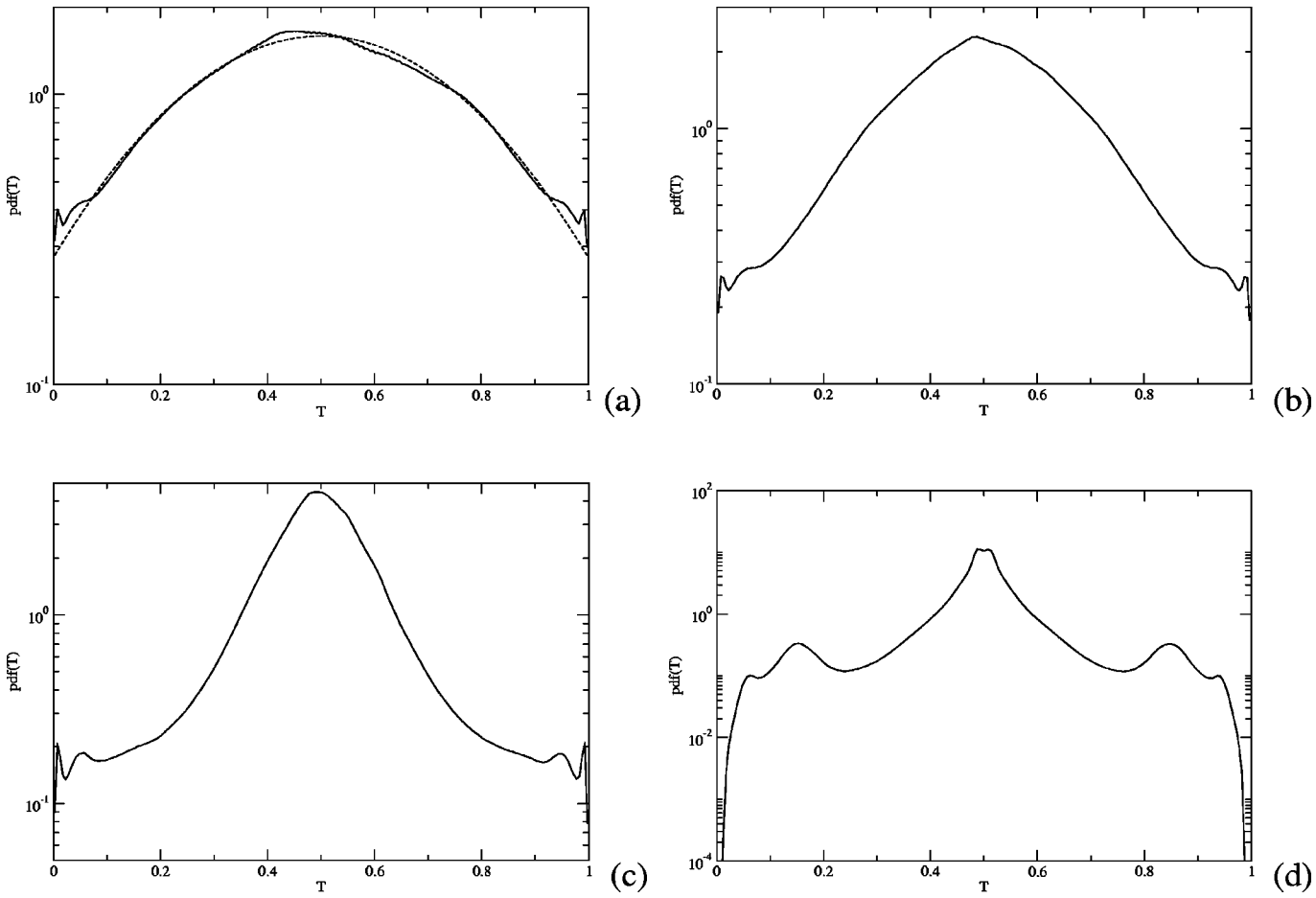

FIG. 3. The spatial temperature probability density function (PDF) averaged in time in a log-lin scale for the Prandtl number (a) Pr $=0.025$ (the dashed line represents the Gaussian fit), (b) Pr$=0.1$, (c) Pr$=1$, and (d) Pr$=100$.

n_i being the number of registrations in the interval T_i, N the total amount of registrations, and Δ is the bin width. The PDF's have been time averaged over time intervals, sufficiently long to exhibit quasistationary behavior. These spatial PDF's should not be mixed up with the PDF's commonly derived from experimental measurements of the temporal evolution of the temperature at fixed points [15–17]. We employ the PDF's as a tool to characterize the spatial structure of the temperature field. For low Prandtl numbers [Pr $=0.025$, Fig. 3(a)] the spatial PDF shows a clear Gaussian shape. For Pr$=0.1$ and Pr$=1$ [Figs. 3(b) and 3(c)] the PDF starts to deviate from a pure Gaussian shape. In the high Prandtl number case [Pr$=100$, Fig. 3(d)] the PDF possesses a more exponentially behavior with long tails. This implies that the temperature field is spatially uncorrelated for low values of the Prandtl number, while the exponential shape at high Pr indicates that the temperature field possesses spatial coherent structures [18]. We will show subsequently that this change of the PDF's is associated with the presence of thermal boundary layers. The change of flow structure with increasing Pr is also revealed in Fig. 4. Here snapshots of streamlines in the horizontal plane $z=0.5$ are displayed. For low Prandtl numbers [Pr$=0.025$, 0.1, and 1, Figs. 4(a)–4(c)] we observe fine structures characterized by small local vortices. At a Prandtl number of Pr$=100$ the vortices have mostly disappeared and a more laminar flow has emerged. In what follows we will demonstrate that the appearance of small horizontal vortices is related to the toroidal component of the flow. Due to incompressibility (**u** is solenoidal) the velocity field can be decomposed into a poloidal and a toroidal component

$$\mathbf{u}=\boldsymbol{\nabla}\times\boldsymbol{\nabla}\times(\phi\mathbf{e}_z)+\boldsymbol{\nabla}\times(\psi\mathbf{e}_z), \tag{7}$$

ϕ, ψ are the poloidal and the toroidal scalar fields, respectively, and e_z is the unit vector in z direction. From the relation between the z component of the vorticity $\omega_z := \partial v/\partial x - \partial u/\partial y$ and the toroidal scalar field ψ

$$\omega_z=-\nabla_h^2\psi, \tag{8}$$

(∇_h^2 denotes the horizontal Laplacian) it is obvious, that ψ describes the horizontal vortices in the flow field, called the toroidal motion. At a first glance, Fig. 4 leaves already the impression that the small scale vortices, i.e., the toroidal motion, gradually decreases with increasing Prandtl number. This result is corroborated in Fig. 5 showing the ratio of toroidal energy E_{tor} and total kinetic energy E_{kin} as a function of the Prandtl number. The total kinetic energy E_{kin} and the toroidal fraction E_{tor} are derived from

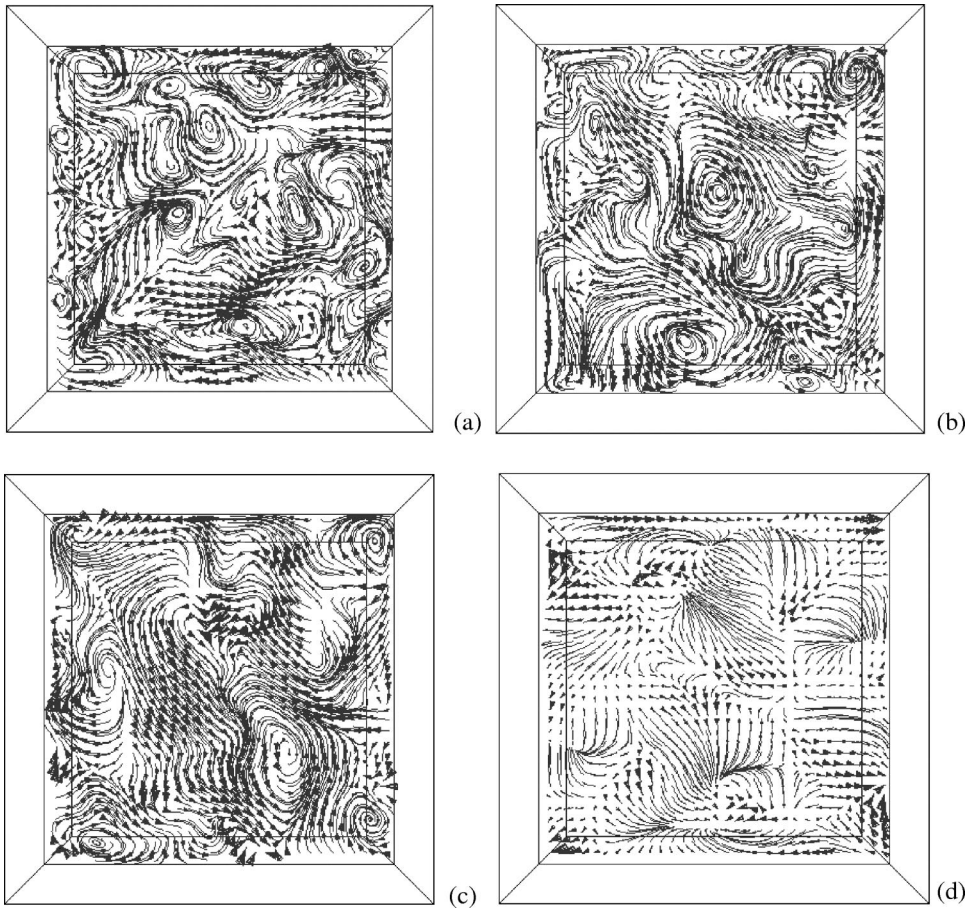

FIG. 4. Snapshots of velocity stream lines projected onto the horizontal plane at $z=0.5$ for different Prandtl numbers: (a) Pr $=0.025$, (b) Pr$=0.1$, (c) Pr$=1$, and (d) Pr$=100$.

$$E_{kin} := \overline{\langle \mathbf{u}^2 \rangle_V}, \quad E_{tor} := \overline{\left\langle \left(\frac{\partial \psi}{\partial x}\right)^2 + \left(\frac{\partial \psi}{\partial y}\right)^2 \right\rangle_V}, \qquad (9)$$

$\langle \cdot \rangle_V$ denotes the spatial mean and — denotes the average in time. In Fig. 5 one can clearly identify two regions: One, for Pr<1, exhibits a virtual constant value of E_{tor} of about 30% of the total kinetic energy. The other, for Pr>1, is characterized by a drastic decrease in the fraction of the toroidal energy with increasing Prandtl number down to less than 1% at Pr$=100$. We reported the Prandtl number dependence of the toroidal motion in a former study [6], where we derived similar results. In that study we employed stress-free conditions, rather than the rigid conditions as used in this study. Thus, it seems to be a fundamental result that, independent of the boundary conditions, the flow contains a strong toroidal component, as Pr is low, while at high Pr it is dominated by poloidal motion. This result is also consistent with theoretical considerations. Taking the curl of the equation of motion [Eq. (1)] it can be shown that in the limit of Pr$\rightarrow\infty$ the toroidal flow component vanishes [19], what is also related to the fact that the Reynolds number Re tends to zero with increasing Prandtl number. We will discuss the Prandtl number dependence of the Reynolds number in Sec. V.

IV. VISCOUS AND THERMAL BOUNDARY LAYERS

The existence of thermal and viscous boundary layers in Rayleigh-Bénard convection is a well known phenomenon and has been thoroughly investigated by different groups [2,20,21]. The behavior of these boundary layers has a strong influence on the global transport processes and such for the Nusselt and the Reynolds number [1,22]. In this section we will discuss the influence of the Prandtl number on the thickness of the viscous and thermal boundary layers. Figure 6

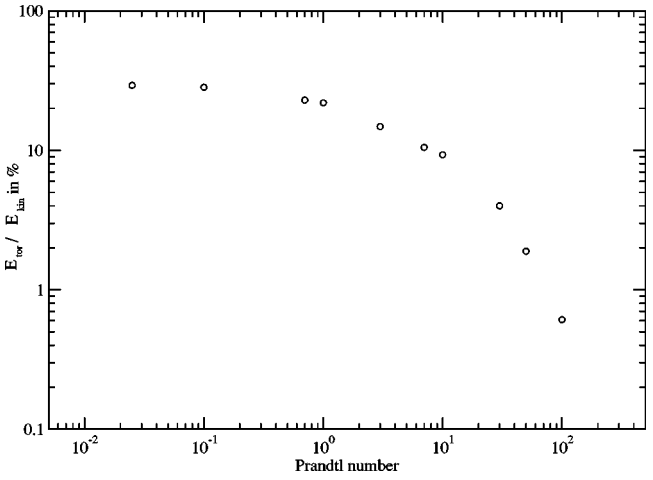

FIG. 5. Ratio of the energy due to toroidal motion to total kinetic energy in percent. For low Prandtl numbers (Pr<1) the fraction of the toroidal flow motion is nearly constant at a value of about 30% whereas for Pr>1 there is a strong decrease in the fraction of the toroidal flow motion with increasing Prandtl number down to less than 1% for Pr$=100$.

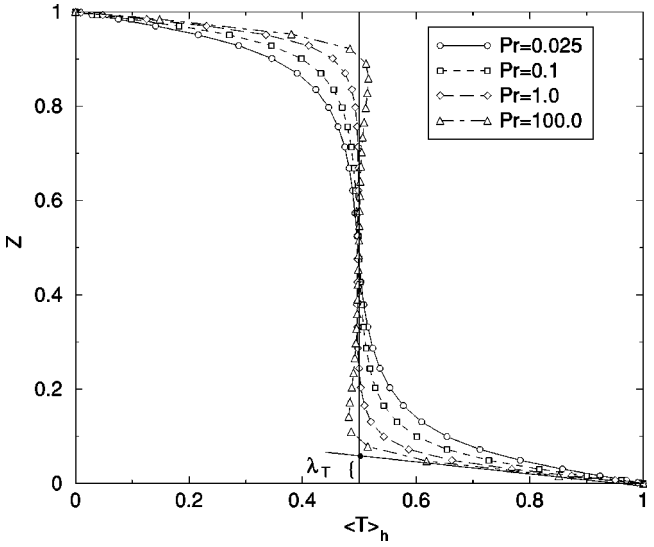

FIG. 6. Temporal averaged depth profiles of the horizontal mean temperature for Pr=0.025,0.1,1,100. For Pr=100 the definition of the thermal boundary layer thickness λ_T is illustrated. λ_T is defined as the depth where a linear fit of the temperature profile near the bottom crosses the mean temperature $T_{mean}=0.5$.

shows time averaged depth profiles of the horizontal mean temperature for different values of the Prandtl number. Two regions can be distinguished. Near the upper and lower boundary layers steep temperature gradients develop adjacent to a well-mixed almost isothermal bulk. Following Verzicco and Camussi [12], we defined the thermal boundary layer thickness λ_T as the depth where a linear fit of the temperature profile near the surfaces crosses the mean temperature $T=0.5$. The vertical heat transport through these thermal boundary layers is mainly conductive because the velocity drops to zero near to the walls. Thus one can deduce an approximative relation between the Nusselt number Nu and the thickness λ_T of the thermal boundary layer [20] given by

$$\lambda_T \approx \frac{1}{2}\mathrm{Nu}^{-1}. \tag{10}$$

Due to no-slip conditions, as applied here, the velocity drops from a characteristic value in the bulk to zero at the boundaries. The layer across which this drop takes place defines the viscous boundary layer. In Fig. 7 depth profiles of the temporally averaged horizontal root-mean-square velocity U_{h_rms} are plotted for various values of the Prandtl number. All profiles show (similar to the temperature profiles) a strong increase in the velocity near the walls with a distinct peak. Similar to Kerr and Herring [1], we defined the thickness ($\lambda_{u,max}$) by the local maximum in the velocity depth profile (cf. Fig. 7). A central assumption in the theory of Grossmann and Lohse [7] is that the viscous boundary layer λ_u approximatively scales as

$$\lambda_u \sim \mathrm{Re}^{-1/2}. \tag{11}$$

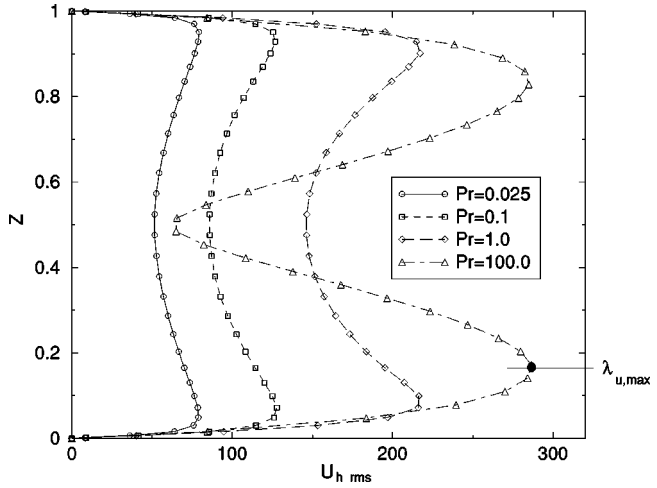

FIG. 7. Temporal averaged depth profiles of the root-mean-square horizontal velocity U_{h_rms} for Pr=0.025,0.1,1,100. In addition, the definition of the viscous boundary layer thickness $\lambda_{u,max}$ is illustrated for Pr=100. $\lambda_{u,max}$ is defined as the distance between the position of the maximum value of U_{h_rms} in the depth profile and the bottom.

They assume a large-scale dominated flow together with a laminar viscous flow of Blasius type in the boundary layer [the derivation of Eq. (11) can be found, e.g., in Landau and Lifshitz [23] §39]. We will return later to the question if these estimates of λ_T [Eq. (10)] and λ_u [Eq. (11)] are in a good agreement with our results. First we will discuss how the viscous and thermal boundary layers are influenced by the value of the Prandtl number. We determined the thickness of the thermal and the viscous boundary layers, according to the definitions, as given above. The results are compiled in Fig. 8, displaying the thicknesses of both types of boundary layers as a function of the Prandtl number. The thermal boundary layer λ_T decreases with increasing Prandtl number

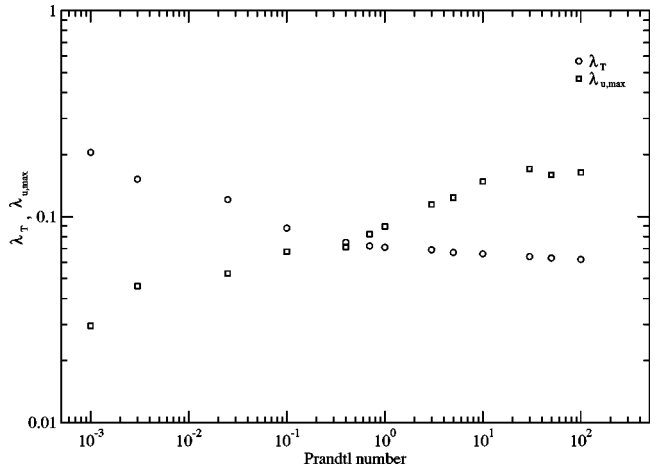

FIG. 8. Thickness of the thermal boundary layer λ_T and the viscous boundary layer $\lambda_{u,max}$ vs the value of the Prandtl number. For low Prandtl numbers the viscous boundary layer is embedded in the thermal boundary layer whereas for high Prandtl numbers the viscous boundary layer exceeds the thermal one with a crossover at around Pr=0.3.

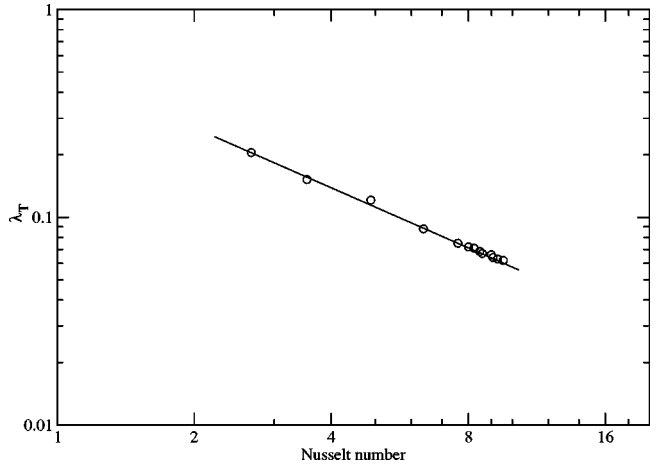

FIG. 9. Thickness of the thermal boundary layer λ_T vs the Nusselt number. The solid line gives a data fit with a power law of $\lambda_T \sim \mathrm{Nu}^{-0.94\pm0.02}$.

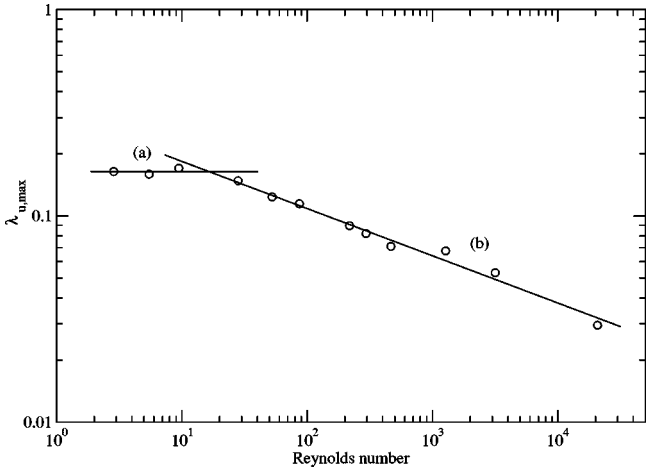

FIG. 10. Thickness of the viscous boundary layer $\lambda_{u,max}$ vs the Reynolds number. Regime (a): The viscous boundary layer thickness is nearly constant. Regime (b): The solid line shows a data fit by a power law of $\lambda_{u,max} \sim \mathrm{Re}^{-0.231\pm0.011}$.

whereas the viscous boundary layer $\lambda_{u,max}$ increases. For low values of Pr the viscous boundary layer is embedded within the thermal boundary layer. At values of Pr around 0.3 we observe a crossover and from that value of Pr the viscous boundary layer is thicker than the thermal one. In a numerical study, but in a spherical shell domain, Tilgner [24] found a similar dependence of the viscous and thermal boundary layers on the Prandtl number. Due to the spherical geometry he finds the thicknesses of the boundary layers to be different at the inner and outer boundary. In our Cartesian geometry the boundary layer thicknesses are for symmetry reasons the same at the lower and upper boundary (cf. Figs. 6 and 7). The viscous boundary layer reaches an asymptotic thickness for $\mathrm{Pr} > 10$ (Fig. 8) and does not further grow. Grossmann and Lohse [8] predicted such a behavior in the large Prandtl number limit. They assume a critical value of the Reynolds number in the case of large Prandtl numbers where the viscous boundary layer does not further increase with increasing Prandtl number.

Now we return to the question if the boundary layers obey the relations as given in Eqs. (10) and (11) which form an essential basis of the theory of Grossmann and Lohse. In Fig. 9 the thickness of the thermal boundary layer is plotted vs the time averaged Nusselt number. A power law of the form $\lambda_T \sim \mathrm{Nu}^{-0.94\pm0.02}$ (the error indicates the standard deviation), being in close agreement with the theoretical prediction of Eq. (10). The dependence of the viscous boundary layer thickness on the Reynolds number is displayed in Fig. 10. We defined the Reynolds number Re over the large-scale horizontal wind by the local maximum of the nondimensional horizontal velocity (cf. Fig. 7)

$$\mathrm{Re} = U_{h\_rms}^{max}/\mathrm{Pr}. \tag{12}$$

As mentioned above we observe a regime for high Prandtl numbers where the viscous boundary layer does not further increase with increasing Prandtl number. The corresponding behavior is displayed in Fig. 10. For low Reynolds numbers (corresponding to high Prandtl numbers) the viscous boundary layer reaches an asymptotic thickness. For higher Reynolds numbers the boundary layer thickness decreases with increasing Re. The transition between those two regimes occurs at a critical Reynolds number Re_{crit} of about 20. A fit of the data provides the power law $\lambda_{u,max} \sim \mathrm{Re}^{-0.231\pm0.011}$ which significantly deviates from the relation given in Eq. (11). This relation forms a central assumption in the theory of Grossmann and Lohse and relies on the existence of a purely laminar flow of Blasius type. This discrepancy was also reported in Ref. [2], an experimental investigation of viscous boundary layer scaling.

The specific definition of the viscous boundary layer by the position of the local velocity maximum, though apparently sensible and as such commonly used, is somewhat arbitrary. Other definitions are feasible and possibly the discrepancy between our numerically determined scaling law and that as assumed in Grossmann-Lohse theory is only a consequence of that specific definition. In order to check this we have employed a second definition $\lambda_{u,lin}$ of the viscous boundary layer. Similar to the thermal boundary layer $\lambda_{u,lin}$ is defined by a linear fit, here of the velocity profile, in the vicinity of the boundary. The intersection of the straight line, resulting from the linear fit, with the vertical tangent to the local maximum in the profile (cf. Fig. 7) defines the boundary layer thickness $\lambda_{u,lin}$. In Fig. 11 the viscous boundary layer thickness $\lambda_{u,lin}$ is plotted as a function of Reynolds number. Similar to the previously employed defined boundary layer, $\lambda_{u,lin}$ is nearly constant for low values of the Reynolds number. In the high Reynolds number regime the data fit provides a power law of $\lambda_{u,lin} \sim \mathrm{Re}^{-0.442\pm0.016}$ which is significantly closer to the scaling based on the assumption of a Blasius-type boundary layer flow. A comparison of Figs. 10 and 11 points out a further discrepancy between $\lambda_{u,max}$ and $\lambda_{u,lin}$. The boundary layer thickness $\lambda_{u,lin}$ turns out to be significantly thinner than the initially considered boundary layer thickness $\lambda_{u,max}$. Consequently, even for high Prandtl numbers the viscous boundary layer remains thinner than the thermal one (cf. Fig. 12). Differently from the boundary layer definition $\lambda_{u,max}$ (Fig. 8), no crossover between $\lambda_{u,lin}$

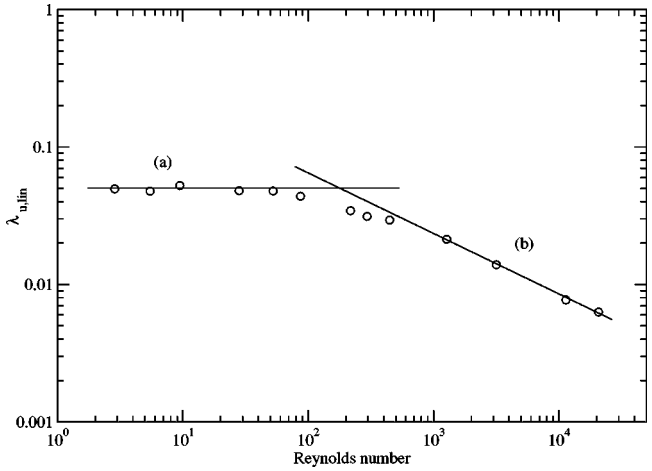

FIG. 11. Thickness of the viscous boundary layer $\lambda_{u,lin}$ vs the Reynolds number. $\lambda_{u,lin}$ is defined by the intersection of the linear fit near the boundary with the tangent to the local maximum in the velocity profile (cf. Fig. 7). For low Reynolds numbers [regime (a)] the viscous boundary layer thickness is nearly constant. In the case of high Reynolds numbers [regime (b)] the viscous boundary layer thickness $\lambda_{u,lin}$ is decreasing as a function of Re following a power law of $\lambda_{u,lin} \sim \mathrm{Re}^{-0.442 \pm 0.016}$.

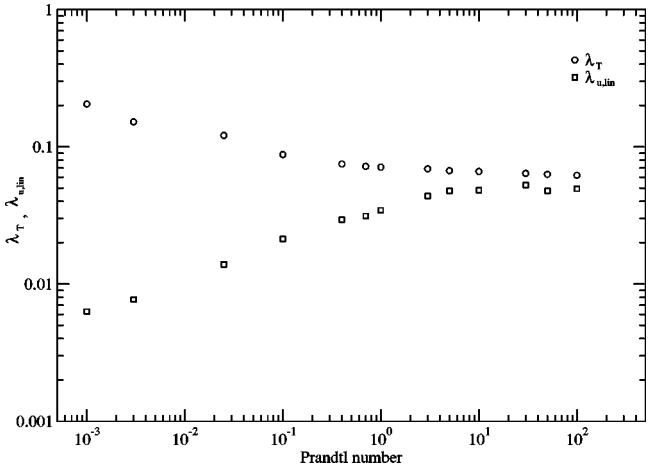

FIG. 12. Thickness of the thermal boundary layer λ_T and the viscous boundary layer $\lambda_{u,lin}$ vs the value of the Prandtl number. Different to the viscous boundary layer definition $\lambda_{u,max}$ (cf. Fig. 8), $\lambda_{u,lin}$ shows no crossover with the thermal boundary layer thickness λ_T in the high Prandtl number case.

and λ_T takes place with increasing Prandtl number. On the one hand the scaling of $\lambda_{u,lin}$ with Re is close to the theoretical assumption of a Blasius type boundary layer flow, on the other hand it does not resemble the theoretical prediction of a changing hierarchy between viscous and thermal boundary layers in the high Prandtl number regime.

At this stage we note that the behavior of both boundary layers based on the definitions $\lambda_{u,max}$, $\lambda_{u,lin}$ are not in full agreement with the Grossmann-Lohse theory.

V. NUSSELT AND REYNOLDS NUMBER VS PRANDTL NUMBER

It is common to describe the state, respectively, the dynamics of thermal convecting systems using global output parameters like the Nusselt and the Reynolds number. The Nusselt number Nu gives the ratio of actual heat transport to the heat transport which would occur in a purely conductive state. The Reynolds number Re measures the ratio of advective momentum transport to the diffusive momentum transport in the equation of motion [Eq. (1)] and indicates how turbulent the velocity field is. Most of the theories of thermal convection assume a simple scaling relation between the global nondimensional output parameters like Nu and Re and the system parameters Ra and Pr. There is known evidence that the particular form of the scaling laws depends on the region in the parameter space, spanned by the system parameters Ra and Pr (for a review see Siggia [25]). Recently Grossmann and Lohse [7,8] have put forward a new theoretical approach which allows them to predict scaling laws for Nu(Ra,Pr) and Re(Ra,Pr) for several flow regimes. They distinguish these regimes by whether kinetic and thermal dissipation occurs mainly in the boundary layer or in the bulk, and by whether the thermal boundary layer is thinner than the viscous one or vice versa. We will now present our results in the light of the theory of Grossmann and Lohse.

The Nusselt numbers obtained from our numerical experiments are plotted in Fig. 13 for different values of the Prandtl number. We can identify two regions with different scaling laws. For low Prandtl numbers, $\mathrm{Pr} \ll 1$, there is a clear increase in the Nusselt number with increasing Prandtl number. In this regime our data are represented by a power law of the form $\mathrm{Nu} \sim \mathrm{Pr}^{0.182 \pm 0.012}$. At a Prandtl number of around 0.3 a transition takes place and beyond that value the Nusselt num-

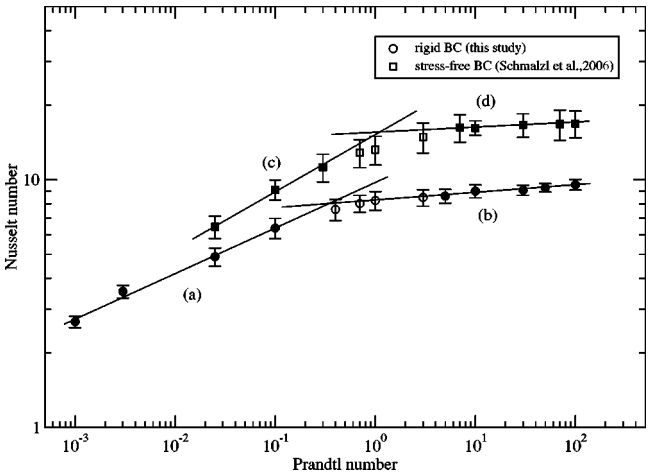

FIG. 13. Values of the Nusselt number averaged in time vs the Prandtl number. The circles represents results from this study with rigid upper and lower boundaries. Squares represent former results derived with stress-free boundary conditions published in Schmalzl *et al.* [6]. In both cases we can identify two different regions in which the increase of the Nusselt number with the Prandtl number follows a different power law [rigid: (a) $\mathrm{Nu} \sim \mathrm{Pr}^{0.182 \pm 0.012}$, (b) $\mathrm{Nu} \sim \mathrm{Pr}^{0.032 \pm 0.003}$, stress-free: (c) $\mathrm{Nu} \sim \mathrm{Pr}^{0.224 \pm 0.017}$, (d) $\mathrm{Nu} \sim \mathrm{Pr}^{0.016 \pm 0.002}$]. The solid lines indicate those fits. Filled circles and squares denote used data to determine fits. The bars represent the standard deviation of the temporal fluctuations.

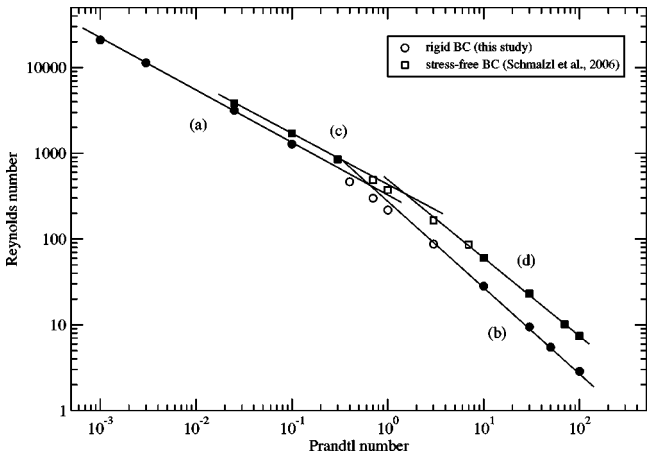

FIG. 14. Values of the Reynolds number vs the Prandtl number. Similar to Fig. 13 the circles represents results of this study (rigid case), whereas the squares denote results of the stress-free case, published in Ref. [6]. In both cases, two regions with different power laws can be identified: rigid case: (a) $\mathrm{Re}\sim\mathrm{Pr}^{-0.607\pm0.012}$, (b) $\mathrm{Re}\sim\mathrm{Pr}^{-0.998\pm0.014}$, stress-free case: (c) $\mathrm{Re}\sim\mathrm{Pr}^{-0.605\pm0.013}$, (d) $\mathrm{Re}\sim\mathrm{Pr}^{-0.916\pm0.014}$.

ber virtually saturates. In fact our data still show a weakly increasing Nu, represented by a power law $\mathrm{Nu}\sim\mathrm{Pr}^{0.032\pm0.003}$. The two regimes are portrayed in Fig. 13 (lower curve). The low Prandtl number branch corresponds to the region II_l in the Grossmann and Lohse picture and is characterized by a thin viscous boundary layer embedded in the thermal one. Dissipation of kinetic energy occurs mainly in the bulk while thermal dissipation takes place in the thermal boundary layers. We have already demonstrated in Fig. 8 that the viscous boundary layer lies in fact within the thermal layer for low values of Pr. For this regime Grossmann and Lohse predict a power law of $\mathrm{Nu}\sim\mathrm{Pr}^{1/5}$ thus being in close agreement with our results. The high Prandtl number branch corresponds to a region which according to Grossmann and Lohse is characterized by dissipation, both thermal and kinetic, taking place mainly in the boundary layers and where no further increase of the viscous boundary layer can be expected. Following the theory Nu does not depend on Pr in this region. Our results reveal that the viscous boundary layer does not further grow with increasing Pr (cf. Fig. 8). The exponent in the power law is very small. Thus we consider our results to be in close agreement with the prediction of Grossmann and Lohse [7,8].

The Reynolds number dependence on the Prandtl number is displayed in Fig. 14 (lower curve). Similar as for the Nusselt number we can define two regions with different scaling behavior, i.e., different power laws in the functional dependence of Re(Pr). For low Prandtl numbers our data yield a power law of $\mathrm{Re}\sim\mathrm{Pr}^{-0.607\pm0.012}$, whereas for high Prandtl numbers the Reynolds number scales with $\mathrm{Re}\sim\mathrm{Pr}^{-0.998\pm0.014}$. These results are almost identical with the predictions of Grossmann and Lohse [7,8]. For small Prandtl numbers (regime II_l) they derive a power law of $\mathrm{Re}\sim\mathrm{Pr}^{-3/5}$ and in the high Prandtl number regime ($I_\infty^>$) a power law of $\mathrm{Re}\sim\mathrm{Pr}^{-1}$. Verzicco and Camussi [12] performed a numerical study in a cylindrical geometry and also report the finding of different regions in the Nu(Pr) and Re(Pr) relations. Quantitatively, however, their results differ from ours. For low values of Pr they obtain an exponent of 0.14 for the Nu(Pr) relation (0.182, this study) and -0.73 for the Re(Pr) relation (-0.607, this study). The differences can probably be addressed to the differences in geometry and boundary conditions. In their study no-slip conditions were applied at the sidewalls while we kept the sidewalls stress-free.

Regardless those differences, a change in the system behavior, reflected by a change in the scaling laws at a Prandtl number of around 1 seems to be an established fact. What is the mechanism behind this transition? Most theories address this transition to a change in the hierarchy between the viscous and thermal boundary layers (e.g., Refs. [26,7]). Namely, they assume that at low values of Pr the viscous layer is nested within the thermal one and that with increasing Pr the thermal boundary layer decreases while the viscous layer grows. A crossover occurs and at large values of Pr the viscous and thermal boundary layer thicknesses reach an asymptotic value. This picture corresponds almost exactly to our observations (cf. Fig. 8), if we consider the viscous boundary layer definition of $\lambda_{u,max}$. Otherwise, the viscous boundary layer based on the definition of $\lambda_{u,lin}$ does not show a crossover with the thermal boundary layer in the high Prandtl number regime and hence contradicts in this point with the theory (cf. Fig. 12). However the change of hierarchy cannot be the cause behind the transition in the scaling laws of Nu(Pr) and Re(Pr). Strictly spoken, the presence of a viscous boundary layer and such also its growth is not necessary for this transition to take place. We have carried out a virtually identical set of experiments, however with stress-free conditions all around the box. Under such circumstances only thermal boundary layers are present, whereas a viscous boundary layer does not exist [6]. The main result of this study is shown in Figs. 13 and 14 (upper curves). For both, rigid and stress-free conditions Nu and Re show quantitatively a very similar functional dependence on Pr. In either case a transition in the Nu(Pr) and Re(Pr) curve is observed and also the describing power laws yield similar values (cf. Figs. 13 and 14). In fact the presence of a viscous boundary layer seems only to affect the actual values of the Nusselt and the Reynolds number, however not the dependence on the Prandtl number. Seemingly the existence of a viscous boundary layer is not a necessary condition for the transition in Nu(Pr) and Re(Pr) to take place. Thus, the mechanism behind the transition in the power laws cannot be the change of hierarchy of viscous and thermal boundary layers. We present an alternative explanation in the following section.

VI. SUMMARY AND DISCUSSION

We have investigated the influence of the Prandtl number on the dynamics of thermal convection. A numerical parameter study has been carried out in a 3D Rayleigh-Bénard configuration for Prandtl numbers $10^{-3}\leqslant\mathrm{Pr}\leqslant10^{2}$. By flow visualization we studied how the spatial structure of the flow is affected by changes in Prandtl number. We further investigated the functional dependence of the global parameters Nu and Re on the Prandtl number. The results are compared

with those from a recent theoretical approach by Grossmann and Lohse [7,8].

We have identified two different regimes:

Low Prandtl number regime ($\mathrm{Pr} \ll 1$). In this regime heat transport is dominated by one large-scale circulation. The regime is characterized by a high ratio of toroidal energy to total kinetic energy. Due to no-slip conditions the strong horizontal wind near the top and the bottom walls creates viscous boundary layers which are embedded within the thermal boundary layers.

High Prandtl number regime ($\mathrm{Pr} \gg 1$). The high Prandtl number regime is characterized by plume dominated heat transport. The flow motion is mainly poloidal and the fraction of toroidal energy on the total kinetic energy tends to zero with increasing Pr. Viscous boundary layers could also be identified in the high Prandtl number regime, but different from the low Prandtl number regime they reach a saturated state with increasing Pr.

In both regimes the power laws for Nu(Pr) and Re(Pr) as derived from our calculations match closely with those obtained theoretically by Grossmann and Lohse for the appropriate regimes. Our experiments also confirm the assumption that for low Pr the viscous boundary layer is thinner than the thermal one and that the viscous boundary layer ultimately stops growing, once a Prandtl number higher than ten is reached. However the behavior of the viscous boundary layer deviates from the theoretical prediction in some sense. The change of hierarchy between thermal and viscous boundary layers, as anticipated from the work of Grossmann and Lohse is only observed for a viscous boundary layer $\lambda_{u,max}$ determined by the local velocity maximum. The boundary layer $\lambda_{u,lin}$, based on a linear fit of the velocity profiles near the boundaries does not show such a crossover. Conversely, $\lambda_{u,lin}$ obeys a power law $\lambda_{u,lin} \sim \mathrm{Re}^{-0.442 \pm 0.016}$, being close to the predicted scaling law of $\lambda_u \sim 1/\sqrt{\mathrm{Re}}$, while $\lambda_{u,max}$ is related to Re by the dependence $\lambda_{u,max} \sim \mathrm{Re}^{-0.231 \pm 0.011}$, thus significantly deviating from the theoretical value. None of the employed velocity boundary definitions yield a behavior that closely resembles the theoretical predictions. Still, the predicted dependences of Nu(Pr) and Re(Pr) agrees well with our results, indicating that the viscous boundary layer does not affect much the scaling laws for Nu(Pr) and Re(Pr). Further strong evidence for the relative insignificance of the behavior of the viscous boundary layer is provided by a set of runs carried out under stress-free, but otherwise identical conditions [6]. In such a configuration, viscous boundary layers do not exist, i.e., their thickness is zero. Despite the absence of viscous boundary layers, Nu and Re show qualitatively the same dependence on Pr as for rigid boundaries. This means that the presence of viscous boundary layers is certainly not a necessary condition for the observed phenomenon to occur and it is indeed unlikely that the viscous layers play an important role in this respect.

In our view it is remarkable that the significance of toroidal motion changes noticeably across the transition from the low to the high Prandtl number branch indicating that the two dynamical regimes are characterized by different transport properties.

ACKNOWLEDGMENTS

The authors profited from discussions during the colloquium ''High Rayleigh Number Thermal Convection'' at the Lorentz Center Leiden, The Netherlands (2003). This work was supported by the ''Deutsche Forschungsgemeinschaft'' (DFG) under Grant No. Ha 1765/7-1.

[1] R.M. Kerr and J.R. Herring, J. Fluid Mech. **419**, 325 (2000).
[2] S. Lam, X.-D. Shang, S.-Q. Zhou, and K.-Q. Xia, Phys. Rev. E **65**, 066306(R) (2002).
[3] G. Ahlers and X. Xu, Phys. Rev. Lett. **86**, 3320 (2001).
[4] S. Ashkenazi and V. Steinberg, Phys. Rev. Lett. **83**, 3641 (1999).
[5] P.-E. Roche, B. Castaing, B. Chabaud, and B. Hébral, Europhys. Lett. **58**, 693 (2002).
[6] J. Schmalzl, M. Breuer, and U. Hansen, Geophys. Astrophys. Fluid Dyn. **96**, 381 (2002).
[7] S. Grossmann and D. Lohse, J. Fluid Mech. **407**, 27 (2000).
[8] S. Grossmann and D. Lohse, Phys. Rev. Lett. **86**, 3316 (2001).
[9] R.A. Trompert and U. Hansen, Geophys. Astrophys. Fluid Dyn. **83**, 261 (1996).
[10] G. Grötzbach, J. Comput. Phys. **49**, 241 (1983).
[11] S. Balachandar and L. Sirovich, Phys. Fluids A **3**, 919 (1991).
[12] R. Verzicco and R. Camussi, J. Fluid Mech. **383**, 55 (1999).
[13] S. Ciliberto, S. Cioni, and C. Laroche, Phys. Rev. E **54**, 5901 (1996).
[14] B. Andreotti and S. Douady, Physica D **132**, 111 (1999).
[15] T.H. Solomon and J.P. Gollub, Phys. Rev. Lett. **64**, 2382 (1990).
[16] X.-Z. Wu and A. Libchaber, Phys. Rev. A **45**, 842 (1992).
[17] A. Bartoloni *et al.*, Int. J. Mod. Phys. C **4**, 993 (1993).
[18] F. Chillá, S. Ciliberto, C. Innocenti, and E. Pampaloni, Nuovo Cimento Soc. Ital. Fis., D **15D**, 1229 (1993).
[19] F.H. Busse, J. Math. Phys. **46**, 140 (1967).
[20] A. Belmonte, A. Tilgner, and A. Libchaber, Phys. Rev. E **50**, 269 (1994).
[21] Y.-B. Xin and K.-Q. Xia, Phys. Rev. E **56**, 3010 (1997).
[22] T.H. Solomon and J.P. Gollub, Phys. Rev. A **43**, 6683 (1991).
[23] L.D. Landau and E.M. Lifshitz, *Fluid Mechanics*, 2nd ed. Course of Theoretical Physics Vol. 6 (Butterworth-Heinemann, Oxford, 1997).
[24] A. Tilgner, Phys. Rev. E **53**, 4847 (1996).
[25] E.D. Siggia, Annu. Rev. Fluid Mech. **26**, 137 (1994).
[26] R.H. Kraichnan, Phys. Fluids **5**, 1374 (1962).